

Broadband and Wide-Angle Invisibility with \mathcal{PT} -Symmetric 2D-Weyl Semimetal

Mustafa Sarisaman^{1, a)} and Murat Tas^{2, b)}

¹⁾*Department of Physics, Istanbul University, 34134, Istanbul, Turkey*

²⁾*Department of Basic Sciences, Altınbaş University, 34217 Istanbul, Turkey*

(Dated: 3 January 2020)

Inspired by the magnificent features of two-dimensional (2D) materials which aroused much of the interest in recent materials science research, we study \mathcal{PT} -symmetric 2D Weyl semimetal (WSM) to reveal the broadband and wide-angle invisible configurations in a \mathcal{PT} -symmetric optical slab system. Desired unidirectional reflectionlessness and invisibility phenomena is obtained by the optimal control of system parameters. We unravel the mystery of broadband and wide-angle invisibility in regular slab materials with finite refractive indices by means of the plenary expressions. We show that materials whose refractive indices relatively small (usually around $\eta = 1$) give rise to quite a lot broadband and wide-angle (almost all incidence angles) invisible configurations. This is not observed with any 2D material other than 2D WSMs. Our findings suggest a concrete expedience to experimental realizations in this direction.

I. INTRODUCTION

\mathcal{PT} symmetry prodigy^{1,2} has raised a remarkable development in quantum mechanics since its early discovery. In particular, its practicable scopes in the fields of quantum optics and condensed matter physics have attracted most of the recent interest in the last decade, and thus it has led to advance numerous studies and applications^{3–20}. It has been shown that the advantage of placing gain and loss layers side by side²¹ inspired several intriguing optical phenomena and devices, such as dynamic power oscillations of light propagation, coherent perfect absorber lasers^{22–27}, spectral singularities^{28–33} and unidirectional invisibility^{6,11,12,50,52–66}. Strictly speaking, a Hamiltonian endowed with \mathcal{PT} -symmetry contains a potential whose feature is displayed by $V(x) = V^*(-x)$ ^{1,2,6,9,10}. In general, complex \mathcal{PT} -symmetric optical potentials can be achieved by means of complex refractive indices, such that their optical modulations in complex dielectric permittivity plane results in both optical absorption and amplification.

Invisibility studies essentially initiated about a decade ago by two separate, but concurrent novel papers by Pendry and Leonhardt^{34,35}, which employ the transformation optics approach. Now, there is a huge body of literature utilizing this method on the invisibility cloaking in photonic systems^{36–49}. Another approach in this field employs the transfer matrix formalism, which is our point of interest in this study. It is revealed that both gain and loss layers are required for an invisible configuration. In this respect, \mathcal{PT} -symmetry helps the related parameters of the system be adjusted in order to realize the invisibility. It is noted that a linear homogeneous slab material equipped with \mathcal{PT} -symmetry can not produce a broadband and wide angle invisibility^{50,51}, i.e. the extend of invisibility remains in rather restricted spectral range and incidence angle. The use of graphene sorts out this problem to some extend^{67,68}, although spectral range could be increased considerably, the range of incidence angle could not

be widened commonly. Therefore, in view of this motivation, we aim to employ 2D Weyl semimetal (WSM) to settle up this problem, and achieve broadband and wide-angle invisibility phenomenon of a \mathcal{PT} -symmetric optically active slab system covered by \mathcal{PT} -symmetric 2D WSM, see Fig. 1.

Recent advances on the 2D materials have triggered development of a vast area of research, not only about their physical properties, but also their applications in various fields, especially in optics^{69–81}. Among all of the 2D materials, graphene has the pioneering role due to its well-documented physical properties and numerous applications^{82–86}. As the family of 2D materials expands to include new members such as 2D WSMs, 2D semiconductors, boron nitride and more recently, transition metal dichalcogenides and Xenos, atomically thin forms of these materials offer endless possibilities for fundamental research, as well as demonstration of improved or even entirely novel technologies^{86–89}. New 2D material treatments could unleash new uses. Exciting properties of 2D materials reveal that they may interact with electromagnetic waves in anomalous and exotic ways, providing new phenomena and applications. Thus, new distinctive studies of invisibility phenomena with 2D materials have arisen. Especially recent works in this field originate essential motivation of our work^{27,90–95}. In this study, we offer one of the potential applications of 2D materials in the invisibility phenomenon together with \mathcal{PT} -symmetry attribute in optical systems.

In our analysis, we present all possible configurations of solutions that support the broadband and wide-angle reflectionlessness and invisibility, schematically demonstrate their behaviors and show the effects of various parameters. In particular, we demonstrate that optimal control of the slab and 2D material parameters, i.e., gain coefficient, incidence angle, slab thickness, and Weyl nodes separation b give rise to broadband and wide-angle invisibility. We present exact conditions and display the role of \mathcal{PT} -symmetric 2D material in the gain adjustment. Our findings can be experimentally realized with ease. Our method and hence results are quite reliable for all realistic slab materials of practical concern.

^{a)}Electronic mail: mustafa.sarisaman@istanbul.edu.tr

^{b)}Electronic mail: tasm236@gmail.com

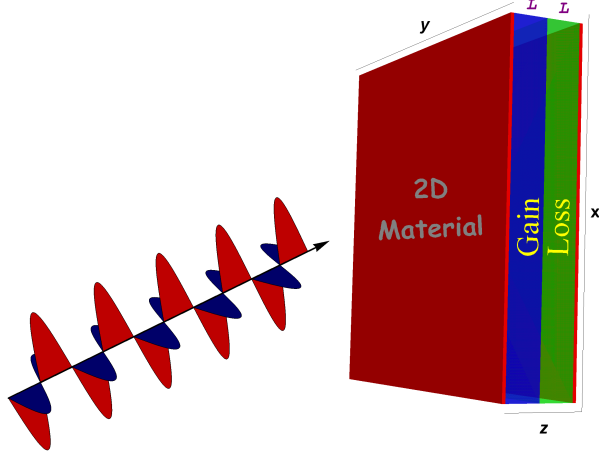


FIG. 1. (Color online) TE mode configuration for the parallel pair of optically active system covered by the 2D material sheets obeying the \mathcal{PT} -symmetry. Wave is emitted on the slab system by an angle θ which is measured from the normal to the surface of 2D material.

II. TE MODE SOLUTION AND TRANSFER MATRIX

Consider a parallel pair of optically active gain and loss slab system covered by the same kind of 2D material at both ends which are enforced to respect the overall \mathcal{PT} -symmetry, as depicted in Fig. 1. The gain and loss regions of slab have the same thickness L , and are restricted to the regions $0 < z < L$ and $L < z < 2L$ with refractive indices n_1 and n_2 respectively. Assuming time-harmonic electromagnetic waves are hitting on the slab, Helmholtz equation associated with TE mode states is expressed as

$$[\nabla^2 + k^2 \mathfrak{z}_j(z)] \vec{E}^j = 0, \quad \vec{H}^j = -\frac{i}{kZ_0} \vec{\nabla} \times \vec{E}^j, \quad (1)$$

where $k := \omega/c$ is the wavenumber, $c := 1/\sqrt{\mu_0 \epsilon_0}$ is the speed of light in vacuum, and $Z_0 := \sqrt{\mu_0/\epsilon_0}$ is the impedance of the vacuum. The index j represents the regions of space respectively corresponding to $z < 0$, $0 < z < L$, $L < z < 2L$ and $z > 2L$, thus $j = 0, 1, 2, 3$. The complex quantity $\mathfrak{z}_j(z)$ is

$$\mathfrak{z}_j(z) := n_j^2 \quad \text{for } z \in z_j. \quad (2)$$

Notice that $n_0 = n_3 = 1$ in vacuum, and hence $\mathfrak{z}_j(z) = 1$ outside the slab. Therefore, TE wave solution of (1) is obtained as

$$\vec{E}^j(\vec{r}) = \mathcal{E}^j(z) e^{ik_x x} \hat{e}_y, \quad (3)$$

where \hat{e}_y denotes the unit vector in y -direction, and k_x and k_z are the components of wavevector \vec{k} in $x-z$ plane. Thus, it is immediate to attain \mathcal{E}^j by use of the Helmholtz equation in (1) as

$$\mathcal{E}^j(Lz) = a_j e^{i\mathfrak{R}_j z} + b_j e^{-i\mathfrak{R}_j z} \quad \text{for } \mathbf{z} \in \mathbf{z}_j. \quad (4)$$

Here a_j and b_j are possibly k -dependent amplitudes, and scaled variables \mathbf{z} and \mathfrak{R} are defined as

$$\mathbf{z} := z/L, \quad \mathfrak{R} := Lk_z = kL \cos \theta. \quad (5)$$

Hence \mathfrak{R}_j is specified by

$$\mathfrak{R}_j := \mathfrak{R} \tilde{n}_j, \quad \tilde{n}_j := \sec \theta \sqrt{n_j^2 - \sin^2 \theta}. \quad (6)$$

Standard boundary conditions at $\mathbf{z} = 0, 1, 2$ yield coefficients a_j and b_j , which include substantial information about the 2D material at the slab ends, and is manifested by the conductivity of the sheets. The conductivity takes a tensorial form and results in the surface current $\vec{\mathcal{J}}_j^{(\ell)} := \sigma_j^{(\ell)} \vec{E}^j$, where σ_j is the conductivity tensor at j -th surface, and ℓ denotes the 2D material type. Our general formalism below is well-established for all 2D materials with only diagonal or off-diagonal conductivity tensor, and hence $\sigma_j^{(\ell)}$ can be regarded as scalar. Here we will specifically consider the 2D WSMs.

We emphasize that the boundary conditions associate the coefficients a_j and b_j , and help to build the transfer matrix which leads to extracting information about the reflection and transmission coefficients of the optical system. Waves on the right-hand side are related to the waves on the left-hand side by the transfer matrix \mathbf{M} as

$$\begin{bmatrix} a_3 \\ b_3 \end{bmatrix} = \mathbf{M} \begin{bmatrix} a_0 \\ b_0 \end{bmatrix}. \quad (7)$$

Hence, components of the transfer matrix in (7) can be obtained as follows

$$M_{\alpha\beta} = \alpha_\alpha \left[U_\beta(u_\alpha^{(2)} + \alpha) e^{i\mathfrak{R}_2} + V_\beta(u_\alpha^{(2)} - \alpha) e^{-i\mathfrak{R}_2} \right], \quad (8)$$

where subindices α, β denote $+, -$, and M_{++} represents the M_{11} component and so forth. Also

$$\alpha_\alpha := \frac{e^{-2i\alpha\mathfrak{R}}}{8}, \quad u_\alpha^{(j)} := \frac{1 + \alpha \sigma_j^{(\ell)}}{\tilde{n}_j},$$

$$U_\alpha := \sum_{\gamma=-1}^{+1} (\tilde{n}_2 + \gamma \tilde{n}_1) (1 + \alpha \gamma u_\alpha^{(1)}) e^{i\gamma\mathfrak{R}_1},$$

$$V_\alpha := \sum_{\gamma=-1}^{+1} (\tilde{n}_2 - \gamma \tilde{n}_1) (1 + \alpha \gamma u_\alpha^{(1)}) e^{i\gamma\mathfrak{R}_1},$$

with $j = 1, 2$. Since the slab system is overall \mathcal{PT} -symmetric, components of \mathbf{M} satisfy the relations in⁹⁶

$$M_{\alpha\beta} \xleftrightarrow{\mathcal{PT}} M_{\beta\alpha}^*, \quad M_{\alpha\beta} \xleftrightarrow{\mathcal{PT}} -M_{\alpha\beta}^*.$$

Notice that $i\alpha$ and $\alpha \sigma_j^{(\ell)}$ are invariant under \mathcal{PT} -symmetry. One thus obtains the following \mathcal{PT} symmetric relations

$$\begin{aligned} n_1 &\xleftrightarrow{\mathcal{PT}} n_2, & \tilde{n}_1 &\xleftrightarrow{\mathcal{PT}} \tilde{n}_2, & \mathbf{a}_+ &\xleftrightarrow{\mathcal{PT}} \mathbf{a}_-, \\ \mathbf{u}_\pm^{(1)} &\xleftrightarrow{\mathcal{PT}} \mathbf{u}_\mp^{(2)}, & \sigma_1^{(\ell)} &\xleftrightarrow{\mathcal{PT}} -\sigma_2^{(\ell)}. \end{aligned} \quad (9)$$

The last relation reveals that currents on the 2D material sheets flow in opposite directions. Hence, the left and right reflection and transmission coefficients are obtained by means of the transfer matrix as

$$\mathbf{R}^l = -\zeta_+ \chi^{-1}, \quad \mathbf{R}^r = \zeta_- \chi^{-1} e^{-4i\mathfrak{R}}, \quad \mathbf{T} = \mathbf{a}_-^{-1} \chi^{-1}, \quad (10)$$

where

$$\zeta_\alpha := U_\alpha(u_{-\alpha}^{(2)} - \alpha)e^{i\tilde{\kappa}_2} + V_\alpha(u_{-\alpha}^{(2)} + \alpha)e^{-i\tilde{\kappa}_2}, \quad (11)$$

$$\chi := U_-(u_-^{(2)} - 1)e^{i\tilde{\kappa}_2} + V_-(u_-^{(2)} + 1)e^{-i\tilde{\kappa}_2}. \quad (12)$$

Notice that these expressions are applicable to all 2D materials having the scalar conductivity $\sigma_j^{(\ell)}$. In this study, we consider 2D WSM² as 2D material which has conductivity $\sigma_j^{(w)}$. For 2D WSM, the conductivity of each sheet is computed by using the Kubo formalism⁹⁷ as

$$\sigma^{(w)} \approx i \int_{\xi < \lambda} \frac{dk_z}{2\pi} \sigma^{2D}(k_z) \xi(k_z) \simeq \frac{ie^2}{\pi h} \ln(2b\lambda), \quad (13)$$

where surface state labeled by k_z is localized near the sheets with a localization length $\xi(k_z) = 2b/(b^2 - k_z^2)$, $\sigma^{2D}(k_z)$ is 2D quantized Hall conductivity, and $\sigma^{2D}(k_z) = e^2/h$, and b is the measure of separation between Weyl nodes given by $b = \mathbf{b}/\hat{e}_z$ in k_z -space. Here the symbol ' \simeq ' is used to imply that real part of $\sigma^{(w)}$ is negligibly small compared to the imaginary part. Therefore, we say that $\sigma^{(w)}$ is pure imaginary as distinct from the case of graphene⁶⁷.

We emphasize that the left/right reflection and transmission coefficients contribute the necessary information about the unidirectional reflectionless and invisible configurations of the optical system, which we explore next.

III. INVISIBILITY CONDITIONS AND RELATED PARAMETERS

An optical system is designed to be left/right reflectionless if $R^{l/r} = 0$ together with $R^{r/l} \neq 0$ is satisfied simultaneously. Moreover, one must provide the condition $T = 1$ to realize the left/right invisibility. Unidirectionally reflectionless condition is achieved once both of the following conditions are satisfied

$$e^{-2i\tilde{\kappa}_2} = \mathcal{F}_\alpha, \quad e^{-2i\tilde{\kappa}_2} \neq \mathcal{F}_{-\alpha}. \quad (14)$$

Here $\mathcal{F}_\alpha := \left[U_\alpha \left(1 - \alpha u_{-\alpha}^{(2)} \right) \right] / \left[V_\alpha \left(1 + \alpha u_{-\alpha}^{(2)} \right) \right]$, and equations with $\alpha = +$ and $-$ correspond to the left and right reflectionlessness respectively. Unidirectional invisibility exists when the condition $T = 1$ is imposed in addition to (14), which yields the condition for left/right invisibility as follows

$$e^{-4i\alpha\tilde{\kappa}} = \mathcal{G}_\alpha, \quad e^{-4i\alpha\tilde{\kappa}} \neq \mathcal{G}_{-\alpha}. \quad (15)$$

where $\mathcal{G}_\alpha := 4\tilde{n}_2^2 \left(1 - \left[u_{-\alpha}^{(2)} \right]^2 \right) / (U_\alpha V_\alpha)$. Eqs. 14 and 15 are in fact complex expressions displaying the behavior of system parameters leading to the unidirectional reflectionlessness and invisibility conditions respectively. Thus, thorough physical consequences of these expressions can be examined by an in-depth analysis. First of all, by virtue of \mathcal{PT} -symmetry relations in (9), we address the following specifications

$$\mathbf{n} := n_1 = n_2^*, \quad \sigma^{(\ell)} := \sigma_1^{(\ell)} = -\sigma_2^{(\ell)*}. \quad (16)$$

We express the real and imaginary parts of refractive index n as $n = \eta + i\kappa$ such that the condition $|\kappa| \ll \eta - 1 < \eta$

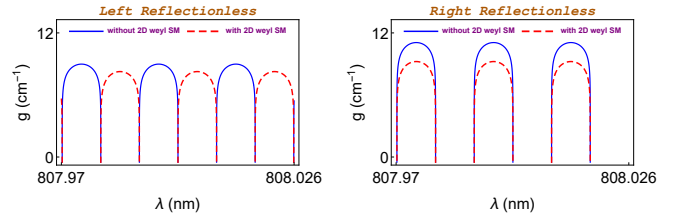


FIG. 2. (Color online) Behavior of the gain g as a function of wavelength λ corresponding to the cases of with and without 2D Weyl SM.

holds by most of the materials. Finally, we introduce another significant parameter, the gain coefficient g as

$$g := -2k\kappa = -\frac{4\pi\kappa}{\lambda}. \quad (17)$$

We replace quantities $\sigma^{(\ell)}$, \mathbf{n} and g into the Eqs. 14 and 15 in order to obtain the reflectionless and invisible behaviors of our optical system. The presence of 2D materials is prevalent explicitly with the term $u_\alpha^{(j)}$ which implicitly contains $\sigma^{(\ell)}$. Thus, desired optimal conditions appear by the selection of most appropriate system parameters. We perform a graphical analysis to seek out the act of each parameter by means of various plots of the gain coefficient g . We take our slab to consist of Nd:YAG crystals⁹ with $\eta = 1.8217$, slab thickness $L = 1$ cm and incidence angle $\theta = 30^\circ$ ⁹⁸. For the 2D WSM, we employ the parameters of $b = 0.05$ Å and wavelength $\lambda = 808$ nm which correspond to the resonance of Nd:YAG crystals⁹. Other parameters are displayed in the figures.

Figure 2 exhibits the behavior of gain coefficient in response to the wavelength λ of incoming waves for the left and right reflectionless cases. We observe that whereas both left and right reflectionless cases in the absence of 2D WSM happen to exist at the same wavelength ranges which form periodically repeated patterns, this turns into a new configuration in the presence of 2D WSM at which left reflectionless wavelength ranges totally shift to the wavelength ranges previously yielding no reflectionlessness while right reflectionless wavelength ranges remain the same. This explicitly shows that placing \mathcal{PT} -symmetric 2D WSM around a \mathcal{PT} -symmetric slab is highly effective in obtaining a drastic change in the gain value. We can not simultaneously observe left and right reflectionlessness in the presence of 2D WSM except for bidirectional reflectionlessness. We also notice that the gain value in case of uni- or bidirectionally reflectionless cases reduces subject to the incident wavelength λ and b -value. We reveal that this engenders a rather intriguing situation that is completely different from graphene. In the case of graphene, specified wavelength range never changes while the gain value reduces similarly to 2D WSM. This causes 2D WSM to show unexpected fascinating features in respect of unidirectional reflectionlessness and invisibility.

A similar behavior is observed in incidence angle vs. gain coefficient plot depicted in Fig. 3. Here we adapt wavelength $\lambda = 808$ nm. Again when the 2D WSM sheets are placed at the ends of the slab, we encounter the left reflectionless pat-

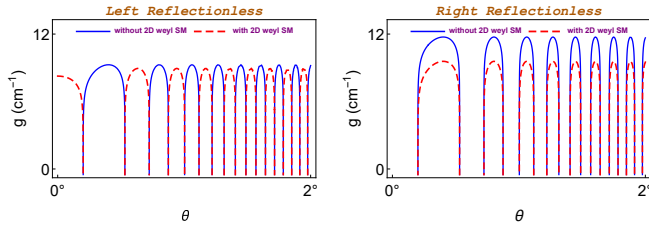


FIG. 3. (Color online) The gain value as a function of incidence angle θ , which yields left and right reflectionless configurations.

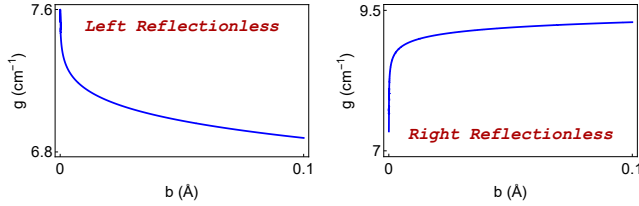


FIG. 4. (Color online) Dependence of the gain upon the parameter b to emanate the left and right reflectionless situations in the presence of 2D Weyl SM.

terns which are fully shifted in the angle ranges that no left reflectionlessness is observed in the absence of 2D WSM. Right reflectionless case yields similar behavior as in Fig. 2. Indeed, we notice that left reflectionlessness occurs at incidence angle $\theta = 0$, which does not appear without the 2D WSM. Corresponding to the same angle ranges, only a certain direction of reflectionlessness is observed.

Figure 4 shows the effect of the parameter b on the gain value in the formation of left and right reflectionlessness. We see that increasing the value of b results in the left reflectionlessness at lower gain values whereas it gives rise to the right reflectionlessness at higher gain values.

Invisible configurations require a tedious analysis because (15) does not provide a unique expression when decomposed into the real and imaginary parts as opposed to the case of reflectionlessness. We represent real and imaginary parts separately and consider intersection points as the corresponding allowed points. Figure 5 displays the left and right invisibility cases corresponding to the allowed gain and wavelength values. Here, we distinguish a couple of conclusions. First one is that left invisibility requires unique and higher gain values at specific wavelength points while the right invisibility could be obtained at very low and extended gain values at designated wavelengths. Our second conclusion is that one can not obtain both of the left and right invisibilities simultaneously with the same gain and wavelength values. This is important because values of the parameters corresponding to the left and right invisibility address unique values, and one must adjust the exact parameters to catch the corresponding directional invisibility.

Figure 6 demonstrates the left and right invisibility configurations corresponding to the gain values as a function of incidence angle θ . Note that not all angles give rise to a unidirectional invisibility, but only certain angles do it. Left in-

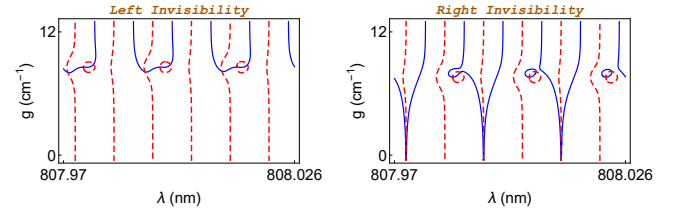


FIG. 5. (Color online) Configurations displaying dependence of the left and right invisibility on the gain coefficient as a function of wavelength in the presence of 2D WSM. Solid blue and dashed red curves respectively represent the real and imaginary parts of (15).

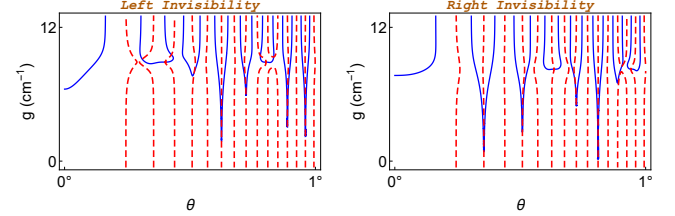


FIG. 6. (Color online) Dependence of the gain on the incidence angle for the left and right invisibility in case of 2D Weyl SM. Again, solid blue and dashed red curves respectively represent the real and imaginary parts of (15).

visibility needs higher gain value compared to the right one. Likewise, left and right invisibility cases are not simultaneously observed at the same incidence angles.

IV. EXACT UNIDIRECTIONAL INVISIBILITY: CONDITIONS FOR BROADBAND AND WIDE-ANGLE

Parameters leading to prescribed reflectionless and invisible potentials guide to construct the associated unidirectional reflectionlessness and invisibility exactly. This is rather simple and smooth mechanism that gives rise to achieve the aimed consequences through the transfer matrix formalism. In this section, we rely on the optimal values of the parameters which give rise to desired wide-angle and broadband invisibility. System parameters dominating the formation of unidirectional invisibility consist of refractive index η which leads to determine the type of slab material to be concealed, slab thickness L , incidence angle θ , wavelength λ , gain coefficient g , and the separation value b of the Weyl nodes. The role of each parameter was exhibited through the relations (14) and (15). Here, in the light of consequences we obtained, we carry out their effects in realizing the wide-angle and broadband invisibility case. First of all, we observe that imposing the condition $T = 1$ into the first two expressions in (10) gives rise to

$$\mathbb{R}^\alpha = -\alpha \zeta_\alpha \mathbf{a}_{-\alpha}, \quad (18)$$

where ζ_α is identified by (11). Here α represents \pm , and denotes the left and right directions respectively. Thus, the left and right invisible configurations are obtained by the condi-

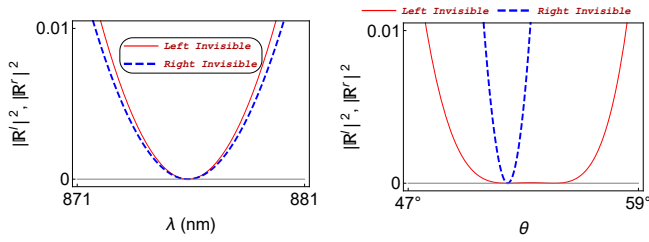


FIG. 7. (Color online) Broadband (left panel) and wide-angle (right panel) invisibilities corresponding to 1% of flexibility for the case of 2D Weyl SM.

tion $\mathbb{R}^\alpha = 0$ once $\mathbb{R}^{-\alpha} \neq 0$ is satisfied. Hence, we should see the behaviors of the parameters in hand to analyze the quantities \mathbb{R}^α . We show the impacts of the effective parameters in plots of $|\mathbb{R}^l|^2$ and $|\mathbb{R}^r|^2$. We employ the optical construction based on Nd:YAG crystals for the slab with $\eta = 1.8217$, $L = 1 \mu\text{m}$, gain value $g = 8 \text{ cm}^{-1}$, $\theta = 30^\circ$ and $b = 0.05 \text{ \AA}$.

In Fig. 7, we present the broadband (left panel) and wide-angle (right panel) invisibility situations within 1% precision. For the broadband case (left panel), right invisibility bandwidth is about $\Delta\lambda \approx 8.4 \text{ nm}$ ranging from $\lambda = 871.7 \text{ nm}$ to $\lambda = 880.1 \text{ nm}$ whereas left invisibility corresponds to the bandwidth $\Delta\lambda \approx 7.7 \text{ nm}$ ranging from $\lambda = 872 \text{ nm}$ to $\lambda = 879.7 \text{ nm}$, which is narrower than the right one. As the precision value increases, broadband invisibility ranges for both left and right directions decrease and approach to each other, leading to a bidirectional invisibility. As for the wide-angle invisibility case, we notice that left invisibility angle range is wider than the right one, at which $\Delta\theta \approx 10.5^\circ$ for the left invisibility case corresponding to the range $(47.9^\circ, 58.4^\circ)$ while it is relatively low for the right invisibility case at which $\Delta\theta \approx 2.5^\circ$ corresponding to the range $(50.9^\circ, 53.4^\circ)$. These broadband and wide-angle invisibility conditions for a regular material type are rather impressive compared to the pure \mathcal{PT} -symmetric slab system and the case with graphene, at which cases it is impossible to obtain such higher values, see^{50,67}.

We question the effects of slab thickness L (left panel) and separation of Weyl nodes b (right panel) on the left and right invisibility in Fig. 8. It is immediate to see from the left panel that broadband and wide-angle invisibility can be recovered at finite sizes apart from smaller thickness values, which is not possible for non-2D WSM cases. This shows that one can achieve broadband and wide-angle invisibility at larger slab thickness values depending on the adjustment of the remaining parameters. This is peculiar to just 2D WSM, and normally not expected for other materials cases. Left panel shows effect of the parameter b such that better results can be obtained with higher b values.

Furthermore, we investigate the extreme cases to accomplish a much broader band and angle widths by managing the type of slab material. It is understood that materials whose refractive indices close $\eta = 1$ display the desired results. For this purpose, we employ aluminum as the slab material whose refractive index is $\eta_{Al} = 1.0972$ ⁹⁹. We choose slab thickness

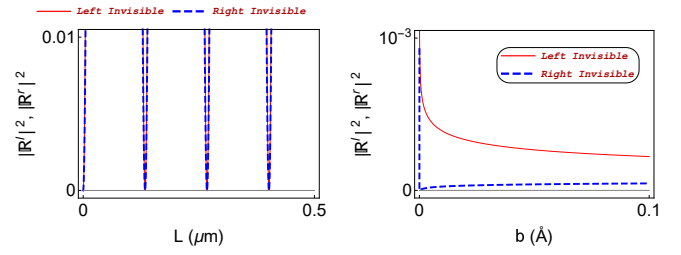


FIG. 8. (Color online) The effect of slab thickness (left panel) and parameter b (right panel) on the broadband and wide-angle invisibility in the case of 2D Weyl SM.

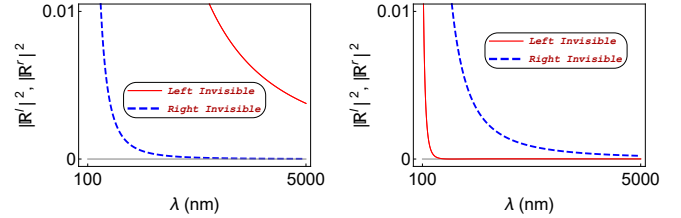


FIG. 9. (Color online) Broadband left and right invisibilities corresponding to the incidence angles of $\theta = 50^\circ$ (left panel), and $\theta = 80^\circ$ (right panel) within 1% of flexibility in the case of aluminum slab covered by a 2D Weyl SM.

as 20 nm , gain $g = 10 \text{ cm}^{-1}$, and b parameter as 0.05 \AA . In Fig. 9, broadband structure of the left and right invisibilities are observed for different incidence angles, $\theta = 50^\circ$ for the left panel, while $\theta = 80^\circ$ for the right one. We notice that left invisibility is highly sensitive to the incidence angle. Its broadband coverage extends from $\lambda \approx 100 \text{ nm}$ to whole low energy regions (Infrared, microwaves and radiowaves) at incidence angle of $\theta = 80^\circ$ while it is ranging from $\lambda \approx 2800 \text{ nm}$ at $\theta = 50^\circ$. However, right invisibility is distinguished from $\lambda \approx 750 \text{ nm}$ at angle of $\theta = 80^\circ$, and $\lambda \approx 365 \text{ nm}$ at angle of $\theta = 50^\circ$. This shows that small incidence angles favor the right invisibility whereas large angles favor the left one. This can be observed in Fig. 10.

In Fig. 10, the left panel corresponds to $\lambda = 1500 \text{ nm}$ and the right one to $\lambda = 5000 \text{ nm}$. We see that as the wavelength decreases swiftly, the angular range of left invisibility gets lowered considerably, and described angular range is restricted to above $\theta \geq 60^\circ$. Once the wavelength increases smoothly, wide-angle invisibility range also increases (at high enough wavelength, one gets all angular range up to $\theta \approx 88^\circ$ as the left invisible region). We notice that right invisibility is easily achieved almost all spectral range at almost all angular ranges (usually up to $\theta \approx 88^\circ$). Thus, one concludes that broadband and wide-angle invisibility is achieved more flexibly for the right invisibility. However one should regard the correct wavelength and angular ranges for the left invisibility.

Figure 11 demonstrates the effect of slab thickness L (left panel) and Weyl node separation b (right panel) on the broadband and wide-angle unidirectional invisibility. We see that even finite values of slab thickness give rise to desired conse-

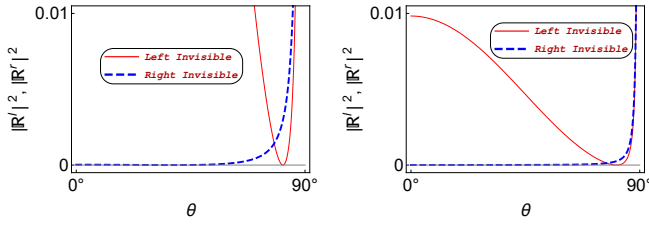


FIG. 10. (Color online) Wide-angle left and right invisibilities corresponding to wavelengths $\lambda = 1500$ nm (left panel) and $\lambda = 5000$ nm (right panel). Slab is made up of aluminum and surrounded by 2D Weyl SM.

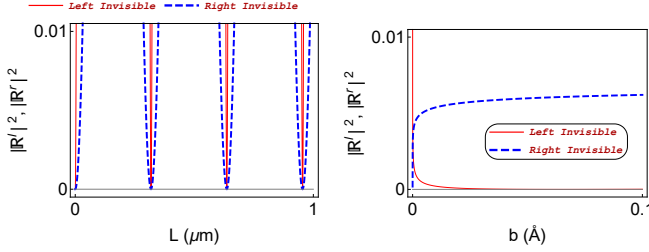


FIG. 11. (Color online) The effect of slab thickness (left panel) and parameter b (right panel) on the broadband and wide-angle invisibility in the case of aluminum slab covered by 2D Weyl SM.

quences. This is rather characteristics of the 2D WSM which is not observed in the case of other material types. The right panel explicitly points out that it is easier to establish left invisibility compared to the right one at usual Weyl node separations. When the Weyl nodes are very close, or very small b values, then pure right invisibility is observed, without allowing the left invisibility.

V. CONCLUDING REMARKS

In this study we draw a general framework towards understanding the broadband and wide-angle invisibility phenomenon of \mathcal{PT} -symmetric optical slabs with the help of \mathcal{PT} -symmetric 2D materials having scalar conductivity. In particular, we focus our attention to 2D Weyl SMs such that its presence gives rise to amazing outcomes. Overall optical system is endowed with the property of \mathcal{PT} symmetry to ensure that essential parameters could be set up properly. No matter which 2D material is placed, we show that the \mathcal{PT} -symmetric slab system results in counter-flowing currents on the surfaces of 2D materials.

Although our expressions holds for all 2D materials with scalar conductivity, in particular we employed 2D WSMs in our analysis because of their distinct properties. We point out that the effect of 2D WSM appears through the function $u_{\alpha}^{(1,2)}$, which is characterized by its scalar conductivity $\sigma^{(w)}$, in the components of transfer matrix, see Eq. 8. In view of the reflection and transmission amplitudes, we obtained relations for the exact unidirectional reflectionless and invisible con-

figurations in (14) and (15), which relate the necessary parameters of the \mathcal{PT} -symmetric optical system covered by the \mathcal{PT} -symmetric 2D WSM. We demonstrated the optimal conditions of the parameters contributing to the screening of unidirectional reflectionlessness and invisibility.

We find out the required gain values, slab thickness, and distance between the Weyl nodes for the unidirectional broadband and wide-angle invisibility. Notice that the same gain values never give rise to simultaneous construct of the left and right invisibilities, as opposed to the case of graphene⁶⁷. In the case of graphene, broadband and wide-angle structures are rather restricted in realistic slab materials unless the refractive index of them approaches $\eta = 1$. Desired phenomenon of unidirectional broadband and wide-angle invisibility is realized at considerably high thickness values. We observe that the Weyl nodes separation b plays a significant role in the broadband and wide-angle invisibility, that favors as large b values as possible. We notice that broadband and wide-angle invisibility is very sensitive to the material type through the refractive index. We performed an extensive analysis of two different kinds of material types, Nd:YAG and aluminum. We show that 2D WSM give rise to the broadband and wide-angle invisible configurations even with the use of usual materials with any refractive index, see Fig. 7. Moreover, when we use a material with a refractive index close to $\eta = 1$, almost full range broadband and wide-angle invisibility is obtained as seen in Figs. 9 and 10. This is quite intriguing and occurs only in the presence of 2D WSM. We expect our results to guide experimental attempts for the realization of broadband and wide-angle invisibility with \mathcal{PT} -symmetric 2D materials.

- ¹C. M. Bender and S. Boettcher, "Real Spectra in Non-Hermitian Hamiltonians Having \mathcal{PT} Symmetry," *Phys. Rev. Lett.* **80**, 5243 (1998).
- ²K. G. Makris, R. El-Ganainy, D. N. Christodoulides, and Z. H. Musslimani, "Beam Dynamics in \mathcal{PT} Symmetric Optical Lattices," *Phys. Rev. Lett.* **100**, 103904 (2008).
- ³A. Mostafazadeh, "Pseudo-Hermitian Representation of Quantum Mechanics," *Int. J. Geom. Meth. Mod. Phys.* **7**, 1191-1306 (2010).
- ⁴C. M. Bender, D. C. Brody, and H. F. Jones, "Must a Hamiltonian be Hermitian?," *Am. J. Phys.* **71**, 1095 (2003).
- ⁵B. Bagchi, and C. Quesne, "sl(2,C) as a complex Lie algebra and the associated non-Hermitian Hamiltonians with real eigenvalues," *Phys. Lett. A* **273**, 285-292 (2000).
- ⁶A. Guo, G. J. Salamo, D. Duchesne, R. Morandotti, M. Volatier-Ravat, V. Aimez, G. A. Siviloglou, and D. N. Christodoulides, "Observation of \mathcal{PT} -Symmetry Breaking in Complex Optical Potentials," *Phys. Rev. Lett.* **103**, 093902 (2009).
- ⁷B. Christian, E. Rüter, K. G. Makris, R. El-Ganainy, D. N. Christodoulides, M. Segev and D. Kip, "Observation of parity-time symmetry in optics," *Nat. Phys.* **6**, 192-195 (2010).
- ⁸L. Feng, M. Ayache, J. Huang, Y. Xu, M. Lu, Y. Chen, Y. Fainman and A. Scherer, "Nonreciprocal Light Propagation in a Silicon Photonic Circuit," *Science* **333**, 729-733 (2011).
- ⁹L. Chen, R. Li, N. Yang, D. Chen, L. Li, "Optical modes in \mathcal{PT} -symmetric double-channel waveguides," *Proc. Rom. Acad., Ser. A : Math. Phys. Tech. Sci. Inf. Sci.* **13**, 46-54 (2012).
- ¹⁰R. Li, P. Li, L. Li, "Asymmetric optical amplifier based on parity-time symmetry," *Proc. Rom. Acad. A* **14**, 121 (2013).
- ¹¹L. Feng, Y. L. Xu, W. S. Fegadolli, M. H. Lu, J. E. Oliveira, V. R. Almeida, Y. F. Chen, A. Scherer, "Experimental demonstration of a unidirectional reflectionless parity-time metamaterial at optical frequencies," *Nat. Mater.* **12**, 108-113 (2013).

- ¹²Y. Shen, X. Hua Deng, and L. Chen, "Unidirectional invisibility in a two-layer non- \mathcal{PT} -symmetric slab" *Opt. Express* **22**, 19440-19447 (2014).
- ¹³A. A. Zyablovsky, A. P. Vinogradov, A. A. Pukhov, A. V. Dorofeenko, and A. A. Lisyansky, " \mathcal{PT} -symmetry in optics," *Phys Uspekhi* **57**, 1063 (2014).
- ¹⁴W.-Xing Yang, A.-Xi Chen, X.-Tao Xie, and L. Ni, "Enhanced generation of higher-order sidebands in a single-quantum-dot-cavity system coupled to a \mathcal{PT} -symmetric double cavity," *Phys. Rev. A* **96**, 013802 (2017).
- ¹⁵J. P. Deka and A. K. Sarma, "Highly amplified light transmission in a parity-time symmetric multilayered structure," *Appl. Optics* **57**, 1119-1126 (2018).
- ¹⁶F. Loran and A. Mostafazadeh, "Perfect broadband invisibility in isotropic media with gain and loss," *Optics Lett.* **42**, 5250-5253 (2017).
- ¹⁷H. Li, M. R. Lopez, Y. Zhu, X. Fan, D. Torrent, B. Liang, J. Cheng, J. Christensen, "Ultrathin acoustic parity-time symmetric metasurface cloak," arXiv:1812.05845 (2018).
- ¹⁸Z. Zhang, M. R. Lopez, Y. Cheng, X. Liu, and J. Christensen, "Non-Hermitian Sonic Second-Order Topological Insulator," *Phys. Rev. Lett.* **122**, 195501 (2019).
- ¹⁹P. Y. Chen and J. Jung, "PT-Symmetry and Singularity-Enhanced Sensing Based on Photoexcited Graphene Metasurfaces," *Physical Review Applied*, **5**, 064018 (2016).
- ²⁰M. Sakhdari, M. Farhat, and P. Y. Chen, "PT-Symmetric Metasurfaces: Wave Manipulation and Sensing Using Singular Points," *New Journal of Physics*, **19**, 065002 (2017).
- ²¹A. Regensburger, C. Bersch, M. A. Miri, G. Onishchukov, D. N. Christodoulides, and U. Peschel, "Parity-time synthetic photonic lattices," *Nature* **488**, 167-171 (2012).
- ²²A. Mostafazadeh, M. Sarisaman, "Spectral singularities of a complex spherical barrier potential and their optical realization," *Phys. Lett. A* **375**, 3387-3391 (2011).
- ²³A. Mostafazadeh, M. Sarisaman, "Optical Spectral Singularities and Coherent Perfect Absorption in a Two-Layer Spherical Medium," *Proc. R. Soc. Lond. Ser. A: Math. Phys. Eng. Sci.* **468**, 3224-3246 (2012).
- ²⁴A. Mostafazadeh, M. Sarisaman, "Spectral singularities and whispering gallery modes of a cylindrical gain medium," *Phys. Rev. A* **87**, 063834 (2013).
- ²⁵A. Mostafazadeh, M. Sarisaman, "Spectral singularities in the surface modes of a spherical gain medium," *Phys. Rev. A* **88**, 033810 (2013).
- ²⁶A. Mostafazadeh, M. Sarisaman, "Lasing-threshold condition for oblique TE and TM modes, spectral singularities, and coherent perfect absorption," *Phys. Rev. A* **91**, 043804 (2015).
- ²⁷A. Mostafazadeh and M. Sarisaman, "Spectral Singularities in the TE and TM modes of a \mathcal{PT} -Symmetric Slab System: Optimal conditions for realizing a CPA-Laser," *Ann. Phys. (NY)* **375**, 265-287 (2016).
- ²⁸M. A. Naimark, "Investigation of the spectrum and the expansion in eigenfunctions of a non-selfadjoint differential operator of the second order on a semi-axis," *Trudy Moscov. Mat. Obsc.* **3**, 181 (1954) in Russian, English translation: *Amer. Math. Soc. Transl.* (2), **16**, 103 (1960).
- ²⁹G. Sh. Guseinov, "On the concept of spectral singularities," *Pramana, J. Phys.* **73**, 587 (2009).
- ³⁰A. Mostafazadeh, "Physics of Spectral Singularities," *Geometric Methods in Physics, Trends in Mathematics*, edited by P. Kielanowski, P. Bieliavsky, A. Odziejewicz, M. Schlichenmaier, and T. Voronov (Springer, Cham, 2015) pp 145-165.
- ³¹A. Mostafazadeh, "Invisibility and \mathcal{PT} symmetry," *Phys. Rev. A* **87**, 012103 (2012).
- ³²S. Longhi, "Invisibility in non-Hermitian tight-binding lattices," *Phys. Rev. A* **82**, 032111 (2010).
- ³³S. Longhi, "Invisibility in \mathcal{PT} -symmetric complex crystals," *J. Phys. A* **44**, 485302 (2011).
- ³⁴J. B. Pendry, D. Schurig and D. R. Smith, "Controlling Electromagnetic Fields," *Science* **312**, 1780-1782 (2006).
- ³⁵U. Leonhardt, "Optical Conformal Mapping," *Science* **312**, 1777-1780 (2006).
- ³⁶D. Schurig, J. J. Mock, B. J. Justice, S. A. Cummer, J. B. Pendry, A. F. Starr and D. R. Smith, "Metamaterial Electromagnetic Cloak at Microwave Frequencies," *Science* **314**, 977-980 (2006).
- ³⁷W. Cai, U. K. Chettiar, A. V. Kildishev, and V. M. Shalaev, "Optical cloaking with metamaterials," *Nat. Photon.* **1**, 224-227 (2007).
- ³⁸J. Li and J. B. Pendry, "Hiding under the Carpet: A New Strategy for Cloaking," *Phys. Rev. Lett.* **101**, 203901 (2008).
- ³⁹R. Liu, C. Ji, J. J. Mock, J. Y. Chin, T. J. Cui and D. R. Smith, "Broadband Ground-Plane Cloak," *Science* **323**, 366-369 (2009).
- ⁴⁰S. Tretyakov, P. Alitalo, O. Luukkonen, and C. Simovski, "Broadband Electromagnetic Cloaking of Long Cylindrical Objects," *Phys. Rev. Lett.* **103**, 103905 (2009).
- ⁴¹W. Li, J. Guan, Z. Sun, W. Wang, and Q. Zhang, "A near-perfect invisibility cloak constructed with homogeneous materials," *Opt. Express* **17**, 26, 23410-23416 (2009).
- ⁴²J. Valentine, J. Li, T. Zentgraf, G. Bartal, and X. Zhang, "An optical cloak made of dielectrics," *Nat. Mater.* **8**, 568-571 (2009).
- ⁴³H. F. Ma, and T. J. Cui, "Three-dimensional broadband ground-plane cloak made of metamaterials," *Nat. Commun.* **1**, 21 (2010).
- ⁴⁴T. Ergin, N. Stenger, P. Brenner, J. B. Pendry, and M. Wegener, "Three-Dimensional Invisibility Cloak at Optical Wavelengths," *Science* **328**, 337-339 (2010).
- ⁴⁵B. Zhang, Y. Luo, X. Liu, and G. Barbastathis, "Macroscopic Invisibility Cloak for Visible Light," *Phys. Rev. Lett.* **106**, 033901 (2011).
- ⁴⁶X. Chen, Y. Luo, J. Zhang, K. Jiang, J. Pendry, and S. Zhang, "Macroscopic invisibility cloaking of visible light," *Nat. Commun.* **2**, 176 (2011).
- ⁴⁷M. Gharghi, C. Gladden, T. Zentgraf, Y. Liu, X. Yin, J. Valentine, and X. Zhang, "A Carpet Cloak for Visible Light," *Nano Lett.* **11**, 2825-2828 (2011).
- ⁴⁸J. Zhang, L. Liu, Y. Luo, S. Zhang, and N. A. Mortensen, "Homogeneous optical cloak constructed with uniform layered structures," *Opt. Express* **19**, 9, 8625-8631 (2011).
- ⁴⁹X. Xu, Y. Fenga, S. Xiong, J. Fan, J. M. Zhao, and T. Jiang, "Broad band invisibility cloak made of normal dielectric multilayer," *Appl. Phys. Lett.* **99**, 154104 (2011).
- ⁵⁰M. Sarisaman, "Unidirectional reflectionlessness and invisibility in the TE and TM modes of a \mathcal{PT} -symmetric slab system," *Phys. Rev. A* **95**, 013806 (2017).
- ⁵¹M. Sarisaman, M. Tas, "Broadband coherent perfect absorber with PT-symmetric 2D-materials", *Ann. Phys. (NY)* **401**, 139-148 (2019).
- ⁵²P. A. Kalozoumis, C. V. Morfonios, G. Kodaxis, F. K. Diakonou, and P. Schmelcher, "Emitter and absorber assembly for multiple self-dual operation and directional transparency," *Appl. Phys. Lett.* **110**, 121106 (2017).
- ⁵³S. Longhi, "Kramers-Kronig potentials for the discrete Schrödinger equation," *Phys. Rev. A* **96**, 042106 (2017).
- ⁵⁴Y. Huang, Y. Shen, C. Min, S. Fan and G. Veronis, "Unidirectional reflectionless light propagation at exceptional points," *Nanophotonics* **6(5)**, 977-996 (2017).
- ⁵⁵A. Mostafazadeh and N. Oflaz, "Unidirectional reflection and invisibility in nonlinear media with an incoherent nonlinearity," *Phys. Lett. A* **381**, 3548-3552 (2017).
- ⁵⁶O. V. Shramkova, K. G. Makris, D. N. Christodoulides, and G. P. Tsironis, "Dispersive non-Hermitian optical heterostructures," *Photonics Research* **6**, A1-A5 (2018).
- ⁵⁷S. S. Deka, S. H. Pan, Q. Gu, Y. Fainman, and A. El Amili, "Coupling in a dual metallo-dielectric nanolaser system," *Optics Lett.* **42**, 4760-4763 (2017).
- ⁵⁸X. Wu, C. Jin, C. Fu, "Eigenvalues analysis for EM waves in anisotropic materials and its applications for unidirectional transmission and unidirectional invisibility," *Optics Communications* **402**, 507-510 (2017).
- ⁵⁹S. Longhi, "A unidirectionally invisible \mathcal{PT} -symmetric complex crystal with arbitrary thickness," *J. Phys. A* **47**, 485302 (2014).
- ⁶⁰A. Mostafazadeh, "Transfer matrices as nonunitary S matrices, multimode unidirectional invisibility, and perturbative inverse scattering," *Phys. Rev. A* **89**, 012709 (2013).
- ⁶¹A. Mostafazadeh, "Unidirectionally invisible potentials as local building blocks of all scattering potentials," *Phys. Rev. A* **90**, 023833 (2014).
- ⁶²B. Midya, "Supersymmetry-generated one-way-invisible \mathcal{PT} -symmetric optical crystals," *Phys. Rev. A* **89**, 032116 (2014).
- ⁶³L. L. Sanchez-Soto, J. J. Monzon, "Invisibility and \mathcal{PT} Symmetry: A Simple Geometrical Viewpoint," *Symmetry* **6(2)**, 396-408 (2014).
- ⁶⁴Z. Lin, H. Ramezani, T. Eichelkraut, T. Kottos, H. Cao, D. N. Christodoulides, "Unidirectional Invisibility Induced by \mathcal{PT} -Symmetric Periodic Structures," *Phys. Rev. Lett.* **106**, 213901 (2011).
- ⁶⁵A. Mostafazadeh, "Perturbative unidirectional invisibility," *Phys. Rev. A*

- 92, 023831 (2015).
- ⁶⁶A. Mostafazadeh, "Active invisibility cloaks in one dimension," *Phys. Rev. A* **91**, 063812 (2015).
- ⁶⁷M. Sarisaman and M. Tas, "Unidirectional invisibility and \mathcal{PT} symmetry with graphene," *Phys. Rev. B* **97**, 045409 (2018).
- ⁶⁸M. Sarisaman and M. Tas, "PT-Symmetric Coherent Perfect Absorber with Graphene," *J. Opt. Soc. Am. B* **35**(9), 001 (2018).
- ⁶⁹F. Schedin, A. K. Geim, S. V. Morozov, E. W. Hill, P. Blake, M. I. Katsnelson, and K. S. Novoselov, "Detection of individual gas molecules adsorbed on graphene," *Nat. Mater.* **6**, 652-655 (2007).
- ⁷⁰R. Stine, J. T. Robinson, P. E. Sheehan, and Cy R. Tamanaha, "Real-Time DNA Detection Using Reduced Graphene Oxide Field Effect Transistors," *Adv. Mater.* **22**, 5297-5300 (2010).
- ⁷¹G. Lu, L. E. Ocola, and J. Chen, "Gas detection using low-temperature reduced graphene oxide sheets," *Appl. Phys. Lett.* **94**, 083111 (2009).
- ⁷²J. T. Robinson, F. K. Perkins, E. S. Snow, Z. Wei, and P. E. Sheehan, "Reduced Graphene Oxide Molecular Sensors," *Nano Lett.* **8**, 3137-3140 (2008).
- ⁷³Y. Shao, J. Wang, H. Wu, J. Liu, I. A. Aksay, and Y. Lin, "Graphene Based Electrochemical Sensors and Biosensors: A Review," *Electroanalysis* **22**, 1027-1036 (2010).
- ⁷⁴Q. He, S. Wu, Z. Yin, and H. Zhang, "Graphene-based electronic sensors," *Chem. Sci.* **3**, 1764-1772 (2012).
- ⁷⁵S. Wu, Q. He, C. Tan, Y. Wang, and H. Zhang, "Graphene-Based Electrochemical Sensors," *Small* **9**, 1160-1172 (2013).
- ⁷⁶J. Duffy, J. Lawlor, C. Lewenkopf, and M. S. Ferreira, "Impurity invisibility in graphene: Symmetry guidelines for the design of efficient sensors," *Phys. Rev. B* **94**, 045417 (2016).
- ⁷⁷S. Chen, Z. Han, M. M. Elahi, K. M. M. Habib, L. Wang, B. Wen, Y. Gao, T. Taniguchi, K. Watanabe, J. Hone, A. W. Ghosh, and C. R. Dean, "Electron optics with p-n junctions in ballistic graphene," *Science* **353**, 1522-1525 (2016).
- ⁷⁸P. -Y. Chen and A. Alu, "Atomically Thin Surface Cloak Using Graphene Monolayers," *ACS Nano* **5**, 5855-5863 (2011).
- ⁷⁹M. Danaeifar and N. Granpayeh, "Wideband invisibility by using inhomogeneous metasurfaces of graphene nanodisks in the infrared regime," *J. Opt. Soc. Am. B* **33**, 1764-1768 (2016).
- ⁸⁰M. Naserpour, C. J. Zapata-Rodríguez, S. M. Vuković, H. Pashaeiadi, and M. R. Belić, "Tunable invisibility cloaking by using isolated graphene-coated nanowires and dimers," *Sci. Rep.* **7**, 12186 (2017).
- ⁸¹G. Oktay, M. Sarisaman, M. Tas, "Lasing with Topological Weyl Semimetal," arXiv:1905.05799 (2019).
- ⁸²A. K. Geim and K. S. Novoselov, "The rise of graphene," *Nat. Mat* **6**, 183-191 (2007).
- ⁸³A. K. Geim, "Graphene: Status and Prospects," *Science* **324**, 1530-1534 (2009).
- ⁸⁴A. H. Castro Neto, F. Guinea, N. M. R. Peres, K. S. Novoselov, and A. K. Geim, "The electronic properties of graphene," *Rev. Mod. Phys.* **81**, 109 (2009).
- ⁸⁵O. V. Yazyev, "Emergence of magnetism in graphene materials and nanostructures," *Rep. Progr. Phys.* **73**, 056501 (2010).
- ⁸⁶T. Smolenski, T. Kazimierzczuk, M. Goryca, M. R. Molas, K. Nogajewski, C. Faugeras, M. Potemski, and P. Kossacki, "Magnetic field induced polarization enhancement in monolayers of tungsten dichalcogenides: effects of temperature," *2D Mater.* **5**, 015023 (2018).
- ⁸⁷D. Jariwala, T. Marks, M. Hersam, "As thin as it gets," *Nat. Mater.* **16**, 155 (2017).
- ⁸⁸A. Gupta, T. Sakhivel and S. Seal, "Recent development in 2D materials beyond graphene," *Prog. Mater. Sci.* **73**, 44-126 (2015).
- ⁸⁹A. Molle, J. Goldberger, M. Houssa, Y. Xu, S. C. Zhang, and D. Akinwande, "Buckled two-dimensional Xene sheets" *Nat. Mater.* **16**, 163-169 (2017).
- ⁹⁰S. Zanolto, F. Bianco, V. Miseikis, D. Convertino, C. Coletti, and A. Tredicucci, "Coherent absorption of light by graphene and other optically conducting surfaces in realistic on-substrate configurations," *APL Photonics* **2**, 016101 (2017).
- ⁹¹F. Liu, Y. D. Chong, S. Adam, and M. Polini, "Gate-tunable coherent perfect absorption of terahertz radiation in graphene," *2D Mater.* **1**, 031001 (2014).
- ⁹²Y. Fan, F. Zhang, Q. Zhao, Z. Wei, and H. Li, "Tunable terahertz coherent perfect absorption in a monolayer graphene," *Opt. Lett.* **38**, 6269-6272 (2014).
- ⁹³S. M. Rao, J. J. F. Heitz, T. Roger, N. Westerberg, and D. Faccio, "Coherent control of light interaction with graphene," *Opt. Lett.* **39**, 5345-5347 (2014).
- ⁹⁴Y. Fan, Z. Liu, F. Zhang, Q. Zhao, Q. Fu, J. Li, C. Gu, and H. Li, "Tunable mid-infrared coherent perfect absorption in a graphene meta-surface," *Sci. Rep.* **5**, 13956 (2015).
- ⁹⁵A. Mostafazadeh, "Spectral Singularities of Complex Scattering Potentials and Infinite Reflection and Transmission Coefficients at Real Energies," *Phys. Rev. Lett.* **102**, 220402 (2009).
- ⁹⁶A. Mostafazadeh, "Generalized unitarity and reciprocity relations for \mathcal{PT} -symmetric scattering potentials," *J. Phys. A* **47**, 505303 (2014).
- ⁹⁷M. Kargarian, M. Randeria, and N. Trivedi, "Theory of Kerr and Faraday rotations and linear dichroism in Topological Weyl Semimetals," *Sci. Rep.* **5**, 12683 (2015).
- ⁹⁸W. T. Silfvast, *Laser Fundamentals*, Cambridge University Press, Cambridge, 1996.
- ⁹⁹A. D. Rakić, A. B. Djurišić, J. M. Elazar, and M. L. Majewski, "Optical properties of metallic films for vertical-cavity optoelectronic devices," *Appl. Opt.* **37**, 5271-5283 (1998).